Antennule morphology and flicking kinematics facilitate odor sampling by the spiny lobster, *Panulirus argus*

Matthew A. Reidenbach*, Nicole George and M. A. R. Koehl

Department of Integrative Biology, University of California, Berkeley, CA 94720-3140, USA

*Author for correspondence at present address: Department of Environmental Sciences, University of Virginia, Charlottesville, VA 22904, USA
(e-mail: reidenbach@virginia.edu)

SUMMARY

Many arthropod olfactory appendages bear arrays of hair-like chemosensory sensillae. Odor molecules in the fluid around the animal must reach the surfaces of those hairs to be sensed. We used the lateral flagellum of the olfactory antennule of the spiny lobster, *Panulirus argus*, as a system to study how the morphology, orientation, and motion of sensilla-bearing appendages affects the small-scale water flow within the hair array. We tested whether antennule flicking enables lobsters to take discrete odor samples by measuring flow fields through an aesthetasc array on a dynamically scaled physical model of a *P. argus* antennule. Particle image velocimetry revealed that the magnitude and duration of velocity through the aesthetasc array during the rapid flick downstroke is just enough to allow complete replacement of the fluid entrained within the hair array. The complex zig-zag arrangement of aesthetascs hairs, combined with their offset orientation along the antennule, generates flow velocities that are uniform along the length of the hairs. This increases fluid exchange during the flick and reduces the boundary layer thickness surrounding the hairs. The return stroke occurs at about a quarter the speed of the flick, but the velocity of the fluid between the aesthetascs is approximately 25 times slower. The retained fluid during the return stroke remains virtually unstirred and sufficient time occurs for odor molecules to diffuse to aesthetasc surfaces.

Key words: lobster, olfaction, antennule, aesthetasc, chemoreception, *Panulirus argus*, Reynolds number, particle image velocimetry.

INTRODUCTION

Many terrestrial and aquatic organisms use their sense of smell to locate food, identify mates, and find suitable habitats. Fluids moving in the environment carry odor molecules across a habitat from their source. Both in terrestrial and aquatic environments, the instantaneous spatial and temporal structure of an odor plume is complex and depends upon how the odors are dispersed by turbulent wind or water flow (Webster et al., 2001; Koehl, 2006). Both field and laboratory measurements of odor plumes show that concentrations of odors are filamentous and highly intermittent, both in space and time, and vary in systematic ways with distance from the odor source (Crimaldi and Koseff, 2001; Rahman and Webster, 2005; Koehl, 2006; Moore and Crimaldi, 2004). These spatial and temporal odor signals are sampled by the olfactory organs (e.g. noses, antennae, antennules) of animals navigating through the environment and can provide information about the nature and location of the odor source (Atema, 1996; Koehl, 2006; Moore and Crimaldi, 2004). The first step in the process of smelling, before neural processing, is the physical capture of odorant molecules from such plumes in the fluid surrounding an animal.

Many animals actively sample odor-bearing fluid from their environments, and such 'sniffing' is an important component of the process of smelling (Schoenfeld, 2006). The purpose of this study was to examine how the structure and odor-capturing movements of an active olfactory organ affect how it takes samples of the fluid around it. Here we focus on the olfactory antennules of the Caribbean spiny lobster, *Panulirus argus* (Latreille).

Sniffing by lobster olfactory antennules

Decapod crustaceans have different types of hair-like chemosensory sensilla on various appendages, including the first antennae ('antennules'), second antennae, mouthparts, claws and walking legs (Moore et al., 1991; Keller et al., 2003). Both behavioral and neurobiological studies are elucidating various roles that these diverse sensilla play in odor recognition and tracking (Steullet et al., 2002; Johnson and Atema, 2005; Schmidt and Derby, 2005; Horner et al., 2007). We used the lateral flagellum of the olfactory antennule of the spiny lobster, *Panulirus argus*, as a system to study how the morphology, orientation, and motion of sensilla-bearing appendages affects the small-scale water flow within the hair array.

The olfactory antennules of decapod crustaceans such as lobsters and crabs, have two branches, called flagella. The lateral flagellum of an antennule bears rows of chemosensory hairs called aesthetascs (Fig. 1) (Koehl, 2006), which contain chemosensory neurons that project to the olfactory lobes of the brain (Steullet et al., 2002; Horner, 2007; Schmidt, 2007). Both the lateral and medial flagella of an antennule also bear other sensilla containing chemosensory neurons that project to the lateral antennular neuropil (Steullet et al., 2002; Schmidt and Derby, 2005; Horner at al., 2007). Although a variety of chemosensory sensilla on the antennules and other appendages are involved in various aspects of food-odor tracking (Keller et al., 2003), the aesthetascs alone appear to be involved in processing odors from conspecifics (Johnson and Atema, 2005; Horner et al., 2007).

Many crustaceans, such as crabs and lobsters (including *P. argus*) sample the odorants in the surrounding environment by flicking the aesthetasc-bearing lateral flagellum of an antennule through the water (Fig. 2). This flicking has been described as "sniffing" (Schmitt and Ache, 1979; Koehl, 2006). Dye studies revealed that water flows through the aesthetasc array during the rapid flick downstroke, and that this water is retained within the array of
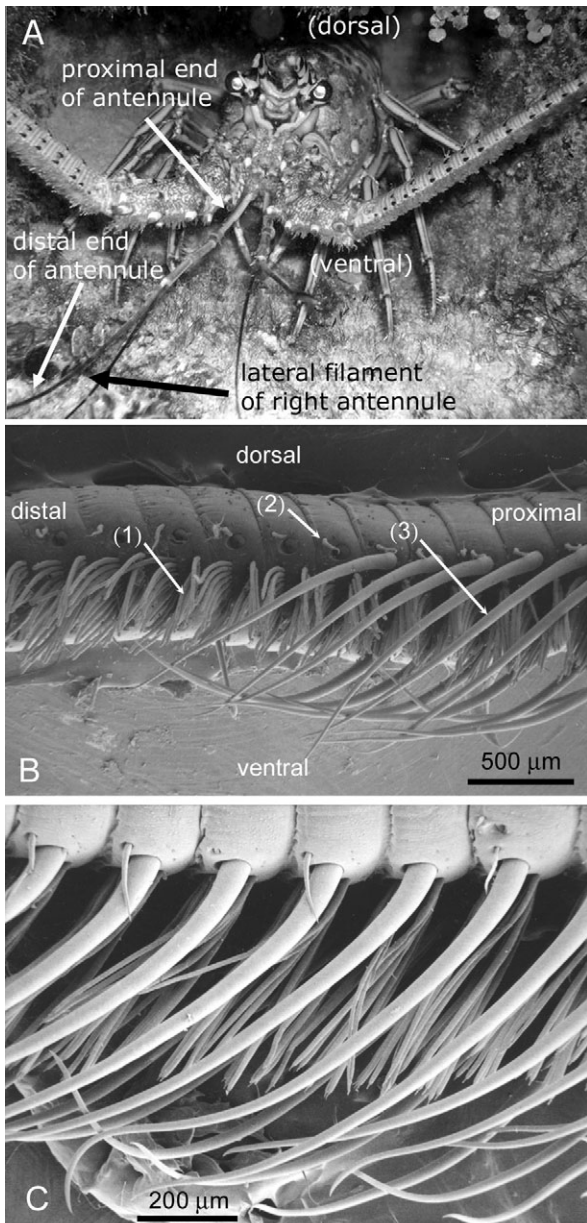
Fig. 1. (A) Face-on view of a spiny lobster, *Panulirus argus*. The arrows point to the lateral flagellum of the antennule bearing rows of aesthetascs. (B) Scanning electron micrograph (SEM) of a three-quarter view of a *P. argus* antennule, showing (1) aesthetascs, (2) mechanosensory hairs and (3) guard hairs. The guard hairs on the left side of the image were removed to show the zig-zag pattern of the tips of the aesthetascs. The aesthetascs and guard hairs line the ventral side of the lateral flagellum. (C) Side view SEM of a lateral flagellum of an antennule. (SEM photos by J. A. Goldman.)
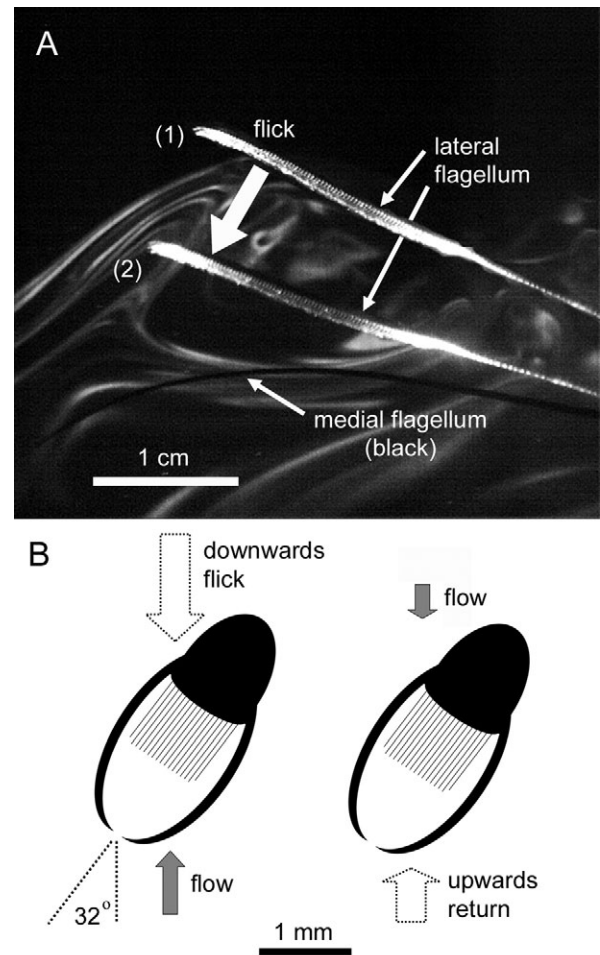

Fig. 2. (A) Side view of video images of the downstroke flick (lasting 100 ms) by the lateral flagellum of a *P. argus* antennule, showing its position at the start (1) and end (2) of the flick as it passes through an odor plume. The lateral flagellum of the antennule appears light because it was flicking in a plane illuminated by a sheet of laser light. The medial flagellum of the antennule, which did not move during the flick, appears black because it was not in the plane illuminated by the laser. The lobster was facing upstream in a flume (flow from left to right) and the antennule was flicking in a turbulent plume of odor mixed with fluorescent dye (fluorescein), which appears as pale filaments swirling in the water around the antennule. (B) Diagram of a cross-section of the lateral flagellum, showing the orientation (angle between dotted lines) of the aesthetascs with respect to the direction of the rapid antennule downwards flick (left diagram) and slower upwards return stroke (right diagram). The direction of water motion relative to the antennule, which changes as a result of the antennular motion is indicated by the solid arrows.

aesthetascs during the slower return stroke (Koehl et al., 2001). Such intermittent flicking has been suggested both to enable lobsters to take discrete samples of odor-containing fluid and, between flick downstrokes, to allow sufficient time for odor molecules trapped in the aesthetasc array to undergo molecular diffusion to the chemosensory cells in the aesthetascs (Koehl et al., 2001). The importance of the dynamics of a flick to how a turbulent odor plume is sampled has also been studied by Crimaldi et al. (Crimaldi et al., 2002), who showed that flicking increases both the number of odor

filaments sampled per time and the probability of sampling an odor filament of high concentration. Furthermore, if flicking does not disrupt the filament structure of an odor plume, it also permits sampling of the spatial structure of the plume along the antennule (Koehl et al., 2001), which may permit animals to use that information in determining the location of the odor source (Webster and Weissburg, 2001).

Approximately 1000–2000 aesthetascs form a dense hair tuft along the distal portion of the lateral flagellum of each antennule

of a *P. argus* lobster (Gleeson et al., 1993). These aesthetascs are attached to the lateral flagellum in transverse rows, but their distal tips are arranged in a zig-zag pattern along the antennule (Grunert and Ache, 1988; Gleeson et al., 1993; Goldman and Koehl, 2001). Each aesthetasc, which is about 0.8 mm long, contains approximately 320 sensory neurons whose dendrites project as a bundle into the hair shaft (Grunert and Ache, 1988). Olfaction occurs when odor molecules, carried by molecular diffusion, diffuse through the cuticle into the lumen of the aesthetasc, and bind to receptors on the outer dendritic segments of an olfactory neuron. The distal 80% of the length of the aesthetasc, which has a thin cuticle, contains only the dendritic segments of receptor cells, and should provide a 'pure' membrane for chemosensory transduction (Grunert and Ache, 1988). When enough odor molecules bind to the receptors on a neuron, the neuron depolarizes (i.e. 'spikes') and the signal is transmitted to the olfactory lobe of the brain (Schmitt and Ache, 1979). How does antennule flicking affect the movements of odor-bearing water around these chemosensory aesthetascs?

The relative importance of viscous to inertial forces in determining flow around a biological structure, such as an aesthetasc, is defined by the Reynolds number (*Re*) as:

$$Re = \frac{UL}{v} , \qquad (1)$$

where U is the velocity of the fluid relative to the structure, L is the characteristic dimension of the structure (e.g. aesthetasc diameter) and v is the kinematic viscosity of the fluid (e.g. sea water). Aesthetascs of *P. argus* operate at low *Re* (Goldman and Koehl, 2001; Koehl et al., 2001), hence the flow is dominated by viscous interactions in the fluid and is laminar. In such flow, there is no turbulent mixing between adjacent fluid layers and molecular diffusion is the only mechanism that transports dissolved substances (e.g. odorants) across streamlines towards or away from the surface of an aesthetasc. Therefore, the rate of arrival of odor molecules to the surfaces of an aesthetasc depends first on the inertially dominated advection of the fluid to the vicinity of the hair and then on the molecular diffusion of odorants from the bulk flow to the surface of the hair (Stacey et al., 2002).

When fluid moves relative to a solid surface, the fluid in contact with the surface does not slip with respect to that surface (i.e. the no-slip condition). Owing to no-slip and to viscous interactions between the fluid molecules, a velocity gradient develops in the fluid between the surface and the freestream flow, forming a boundary layer. The slower the flow, the thicker the boundary layer that forms. Typically, the larger the *Re*, the thinner the velocity boundary layer is relative to the size of a structure (Schlichting and Gersten, 2000), such as a hair. Therefore, the higher the *Re* of the hairs within an array of hairs, the greater the fluid transport through the gaps between hairs in that tuft (e.g. Cheer and Koehl, 1987). The advective transport in the vicinity of each hair is a function of how much fluid passes through, rather than around, the array (Loudon et al., 1994). Gleeson et al. (Gleeson et al., 1993) proposed that the zig-zag arrangement of the aesthetasc tips on the antennules of *P. argus* allows fluid to be channeled between neighboring aesthetascs.

Kinematics of antennule flicking

Lobsters typically flick the lateral flagellum of their antennule several times in a row and then pause for a short time period (usually a few seconds or less) before executing another series of flicks. Average flicking frequencies measured for undisturbed lobsters were between 0.4 and 1.5 Hz (Gleeson et al., 1993; Goldman and Koehl,

2001). When odors from food were present, the lobsters flicked much quicker, with measured flicking frequencies up to 3.5 Hz. Velocities and *Re* of the aesthetascs during the flick downstroke and upstroke were measured by Goldman and Koehl (Goldman and Koehl, 2001). For both undisturbed lobsters and those that smelled food odors, average peak velocities were measured at $0.09\pm0.01\,\mathrm{m\,s^{-1}}$ during the downstroke flick, with a mean velocity of $0.06\pm0.01\,\mathrm{m\,s^{-1}}$. During the upstroke return, mean velocity was $0.02\pm0.01\,\mathrm{m\,s^{-1}}$ (*N*=15 individuals). The average duration of the downstroke flick was 0.10 s, while the upstroke was more variable in duration, but on average lasted 0.34 s. Using the dimension of the aesthetasc hair as the length-scale, the Reynolds number for the maximum speed during the downstroke was *Re*=2±0.4, with a mean *Re*=1±0.5. During the upstroke, the mean *Re*=0.5±0.3. These *Re* values did not vary significantly with carapace length. Since the aesthetascs of the antennules operate at a range of *Re* values of order 1, the amount of fluid passing through the array of aesthetasc hairs should be sensitive to speed and hair spacing and may enhance their ability to take discrete water samples with each flick (Koehl, 1995).

Morphology of antennule

The morphology of the *P. argus* antennule has been described in detail for both adults and juveniles in Goldman and Koehl (Goldman and Koehl, 2001). The scaled model used in our study was based on the characteristics of a flicking adult lobster whose mean antennule width is 1 mm and aesthetasc hair diameter is 22 μm. The rows of aesthetasc hairs are characterized by having an average density of 10 hairs per row and aligned in a zig-zag pattern at the tips of the aesthetascs. The aesthetascs do not point directly into the flow but are oriented at a mean angle of 32°±4° to the flow during the downward flick, and during the upward return stroke are at an obtuse angle of 148°±4° to the flow as the antennule moves in the opposite direction from that of the flick (shown in Fig. 2B). For all measured antennules in Goldman and Koehl (Goldman and Koehl, 2001), the morphologic parameters such as aesthetasc size, spacing and orientation did not vary significantly with respect to carapace length, suggesting that these parameters were maintained over a range of body sizes.

Dynamically scaled physical models

Dynamically scaled physical models are useful tools for studying fluid flow around biological structures that are too large or small to be easily measured in the laboratory. If the biological structure and model are geometrically similar and their motion is characterized by the same Reynolds number, then the ratios of the velocities and the forces in the fluid around the model and the real structure are the same (Loudon et al., 1994; Mead et al., 1999). Physical models also permit the morphology and the kinematics of the structure to be modified so that their consequences to fluid flow around the structure can be explored.

Objectives

We used large dynamically scaled physical models of the lateral flagellum of the olfactory antennule of a spiny lobster, *Panulirus argus*, to determine how the kinematics of flicking and the morphology of the antennule affect flow patterns through the array of chemosensory aesthetascs on the antennule. The specific questions we addressed were:
(1) What are the water velocities through the zig-zag array of aesthetascs during the rapid flick downstroke *versus* during the slower return stroke? Do the antennules 'sniff' (take discrete samples of water in space and time)?

(2) How does the velocity (*Re*) of the flick and of the return stroke affect the water velocities through the array of aesthetascs?

(3) How does the orientation of the aesthetascs relative to the direction of motion of the flicking antennule affect water penetration into the array of aesthetascs?

(4) How does the cage of guard hairs (Fig. 1) around the aesthetasc array affect the water flow through the array?

(5) What are the water velocities encountered by the mechanosensory hairs on the lateral flagellum of an olfactory antennule during the flick downstroke and return stroke?

These fluid flow data not only enable us to assess ways in which antennule morphology and motion affect how such an olfactory organ samples the surrounding water, but also provide the flow velocity fields necessary for future development of a three-dimensional mathematical model of odor transport *via* advection and molecular diffusion to the surfaces of aesthetascs (e.g. Stacey et al., 2002) to determine how flicking affects the kinetics of odorant arrival at these chemosensory hairs.

MATERIALS AND METHODS
Antennule model

In order to make detailed flow measurements through the chemosensory hair array of the *P. argus* antennule, we made a 40:1 geometrically scaled model of the aesthetasc hair array, guard hairs and antennule (Fig. 3). This model consisted of a section of the lateral flagellum of the antennule bearing 15 rows of aesthetascs, containing 10 aesthetascs per row. Each aesthetasc was positioned in the correct orientation and angle to geometrically match measurements obtained from scanning-electron micrograph (SEM) images of real antennules by Goldman and Koehl (Goldman and Koehl, 2001). Relevant morphological and kinematic parameters of the model and real antennule are compared in Table 1. The antennule model was made out of modeling clay (Sculpey© compound, Polyform Products Co., Estes Elk Grove Village, IL, USA), while the aesthetasc and guard hairs were made out of borosilicate glass (Pyrex©, Corning Inc., Lowell, MA, USA) by heating and then shaping the glass to the correct geometry. Once shaped, the hairs were embedded into the clay compound and then kiln dried. For real antennules, no flexing of the guard hairs have been reported during a flicking sequence, whereas for the aesthetascs, Gleeson (Gleeson et al., 1993) reported that only a very slight deflection occurs at the tip (~2.5%) during a flick. Therefore, we constructed our model from materials that are structurally rigid and do not flex during typical flicking behavior.

Experimental apparatus

The tow tank in which experiments were performed was a 250 l tank (100 cm long, 50 cm wide, and 50 cm tall) filled with mineral oil (Fig. 4). The mineral oil had a viscosity of 0.049 Pa s, measured to the nearest 0.002 Pa s with a viscometer (Brookfield Inc., Middleboro, MA, USA) at 25°C. The density of the mineral oil was 840 g l^{-1}. The mineral oil was seeded with 11 µm silver-coated hollow glass spheres (Potter Industries, Malvern, PA, USA), which were slightly denser than the mineral oil, but sank at a velocity less than 1 mm s^{-1}. Since most of the experiments lasted less than 30 s, the sinking of particles did not have any measurable effect on the velocity calculations. The model was towed along the long axis of the tank using a programmable stepper-motor (Daedal Inc., Irwin, PA, USA single-axis microstepping positioning system MC6023) attached to a rail traverse (for details, see Loudon et al., 1994). The speed of the stepper-motor, and thus the towing speed of the model could be controlled by voltage signals sent from a computer. A 20 cm wide by 3 mm thick laser sheet was generated using an array of seven 670 nm laser diodes with an output power of 7 mW each (World Star Tech, North York, ON, Canada). Attached to each laser was a 30° cylindrical beam expander to create the 3 mm thick light sheet. These lasers were aligned horizontally along a rigid plate and mounted to an adjustable microscope stand which could be adjusted vertically to an accuracy of 0.2 mm. The tank of mineral oil was located in a temperature-controlled room away from windows and the temperature was monitored each day to ensure that the density and viscosity of the oil remained constant. Before each experiment, the oil in the tank was stirred to ensure an even suspension of particles, and the fluid was allowed to come to rest so that no fluid motion in the tank occurred before the start of the experiment.

Since this experiment was conducted within an enclosed tank, side walls can affect the flow around low Reynolds number objects even when they are many diameters away from the side walls (Loudon et al., 1994). To ensure minimal interaction with the walls of the tank, particle velocities next to the wall were imaged during the forward and return strokes of the model. No flow interaction with the wall was observed indicating that wall interaction with the
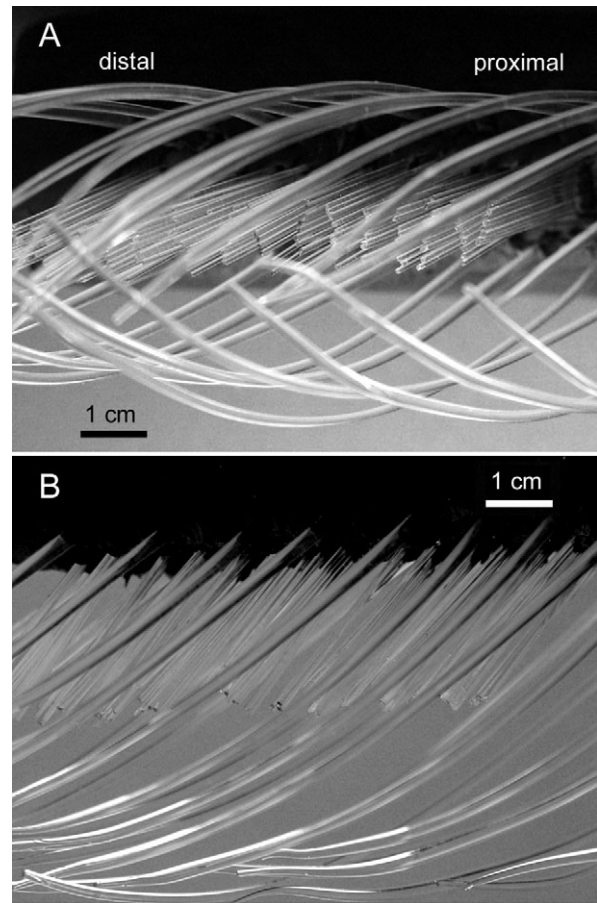

Fig. 3. (A) Ventral and (B) side views of the scaled model (40:1) of the midsection of the lateral flagellum of the antennule of a *P. argus*. The distal end of the antennule is to the left, and proximal end is to the right in the image. The guard hairs and aesthetascs were made from Pyrex© glass to match the index of refraction of mineral oil used as the viscous fluid in the towing tank. The lateral flagellum of the antennule to which the hairs were attached was fabricated using Sculpy© modeling compound.

model was minimal. As a further test, a rule of thumb for estimating when wall effects can be ignored (Vogel, 1994) is:

$$\frac{y}{L} > \frac{20v}{LU} , \qquad (2)$$

where y is the distance to the wall, L is the characteristic diameter of the antennule, U is the velocity of the body relative to the fluid and wall, and v is the kinematic viscosity of the fluid. For our experimental setup, $L=0.04$ m (diameter of the antennule), $U=0.058$ m s^{-1} (slowest towing speed of model, during the return stroke), and $v=5.8\times10^{-5}$ m^2 s^{-1}. For the diameter of the antennule, the model needs to be 2 cm away from the wall for wall effects to be safely ignored. Our model was at a minimum $y=15$ cm away from either wall, indicating that wall effects were negligible.

In order to make velocity measurements within the aesthetasc hair array using particle image velocimetry it was essential to have a direct line-of-sight from the laser light sheet to the camera. To obtain this, the aesthetasc and guard hair array of the model was constructed specifically from Pyrex® glass because it has an index of refraction of 1.47. This matches the index of refraction of mineral oil (1.46) which made the model fully transparent within the mineral oil such that no refraction of emitted light from the laser beams between the oil and glass model occurred. The guard and aesthetasc hair arrays were essentially 'invisible' within the mineral oil.

The model was towed at a velocity to match the Re of the real antennule during the flick and return strokes (with a mean peak $Re=2.0$ during the flick and $Re=0.5$ during the return). The mean aesthetasc diameter of the model was 1 mm, which was used as the characteristic length-scale for Re scaling (Eqn 1). The model was towed at 14.5 cm s^{-1} in the forward motion to obtain a $Re=2.0$ for the flick stroke, and at 3.5 cm s^{-1} for the return stroke to obtain $Re=0.5$. Image recordings were only made when the model was towed within the center of the tank, minimizing the effects of the end wall (Loudon et al., 1994).

Images were obtained at 60 frames per second using a Redlake MotionScope PCI 1000s camera (Redlake Inc., Tucson, AZ, USA) mounted directly above the tank and attached to a motorized traverse. Each image had a resolution of 480 by 420 pixels. Images were processed using particle image velocimetry (PIV) software (MatPIV 1.6.1) written for Matlab® (Sveen, 2004) from a PIV method developed by Cowen and Monismith (Cowen and Monismith, 1997). This software divided each frame of each run into an array of 'interrogation sub-windows' and calculated the most probable displacements of particles in successive pairs of frames using cross-correlation analysis. The final output from the software produced a horizontal and vertical velocity estimate for every 8 by 8 pixel sub-window, giving 59 by 51 velocity measurements per image pair. For each towed experiment we collected 31 images across a transect, generating 30 image pairs. Each experiment was repeated three times for a total of 90 distinct image pairs in which velocities were computed. Means and standard deviations are reported using these 90 independent velocity measurements. To determine spatial
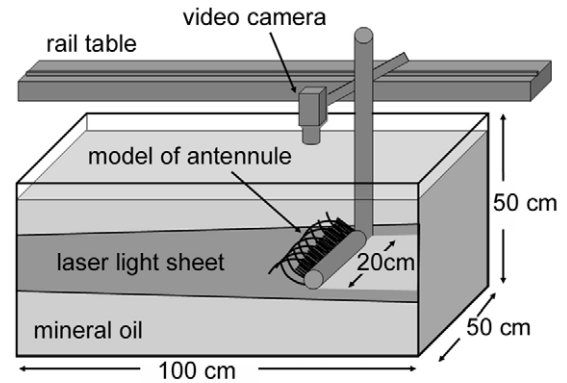

Fig. 4. Schematic diagram of towing-tank. The model of the antennule was attached to a computer-controlled motorized rail table (Daedal MC6023) positioned over the top of the tank and towed through the mineral oil. Neutrally buoyant marker particles (Potter Industries© 11 μm silver-coated hollow glass spheres) in the mineral oil were illuminated by a sheet of laser light and imaged using a Redlake Motionscope PCI 1000s video camera at 60 frames per second. The camera was mounted directly above the tank on the same towing rig as the model, and thus captured images of the particle motion relative to the model. The model was towed in both a horizontal (as shown) and vertical orientation. Towing the model from right to left simulates an antennule in the 'downward' flicking orientation, while a slower tow from left to right simulates an antennule in the 'upstroke' return orientation.

variability of velocities within the aesthetasc array, multiple transects were made by adjusting the location of the laser sheet relative to the model in 1 mm increments. In total, 20 transects were conducted spanning a 20 mm distance along the length of the aesthetasc model.

Accuracy of the PIV measurements was estimated by towing the camera at known speeds with no antennule model attached. For the framing rate used, the accuracy of the velocity measurements were found to improve with slower particle motions. Overall, the relative accuracy of reported velocities, U, are ±6%. Velocities were obtained scaled to the antennule model. All velocities and size scales reported herein have been re-scaled to match the actual velocities and dimensions of a real flicking lobster antennule.

RESULTS
Kinematics of the flick *versus* return stroke
PIV velocity trajectories for the downward flick and return strokes of the *P. argus* antennule are shown in Fig. 5A and Fig. 5B respectively. During the downstroke flick, the fluid velocity passing around the antennule is equivalent to that of the flick speed of 9 cm s^{-1}. Within the guard hair array, but outside the region encompassing the aesthetasc array, the velocity magnitude is reduced to 4.2±0.3 cm s^{-1} and the direction of flow changes to be perpendicular to the aesthetasc hairs. Flow along the ventral edge between the guard hair array and the antennule [labeled as (1) in

Table 1. Morphologic and kinematic parameters of the lateral flagellum of a *Panulirus argus* antennule and the dynamically scaled antennule model used in our experiments

	Antennule diameter (mm)	Guard hair diameter (μm)	Aesthetasc diameter (μm)	Aesthetasc length (μm)	Fluid viscosity (m^2 s^{-1})	Flick velocity (cm s^{-1})	Return velocity (cm s^{-1})	*Re* flick	*Re* return
P. argus antennule*	1±0.2	60±9	22±3	720±50	1.0×10^{-6}	9±1	2±1	2	0.5
Model	40±5	2.4×10^3	800±100	2.9×10^4	5.8×10^{-5}	14.5	3.5	2	0.5

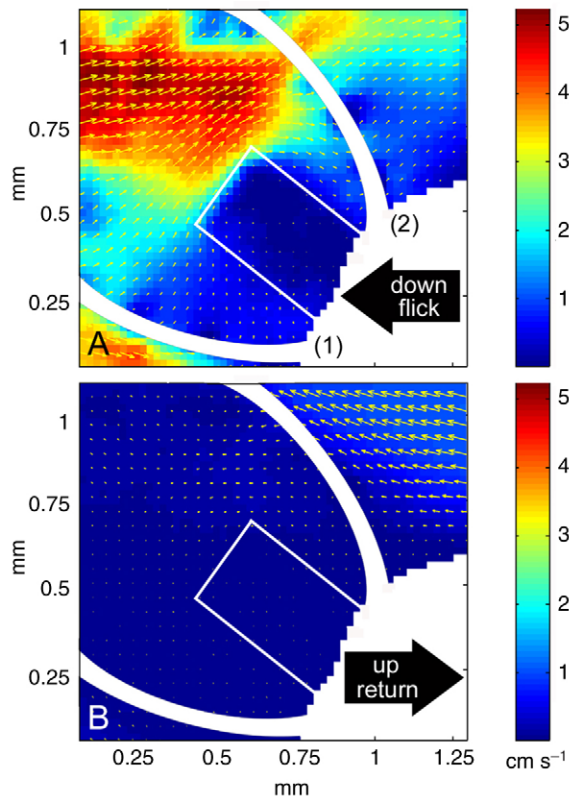*Data from Goldman and Koehl (Goldman and Koehl, 2001). Values are means ± 1 s.d.

Fig. 5. PIV measurements of water velocities relative to a dynamically scaled model of the midsection of the lateral flagellum of the antennule of a *P. argus* during (A) the downward (to the left) flick and (B) the upward (to the right) return stroke. Black arrows indicate direction of antennule motion. Small yellow arrows in the fluid represent the water velocity vectors relative to the antennule lateral flagellum. The model operated at the same Re as the real antennule, and the velocities shown here have been converted to the velocities that would occur relative to the real lobster antennule, which flicks downward at $9\,cm\,s^{-1}$ and returns upward at $2.0\,cm\,s^{-1}$. Background color indicates velocity magnitude. Velocities were computed as the average of 90 measurements at each location. The locations of the guard hairs are shown by wide white curves, and of the aesthetascs by a box outlined with a narrow white line. In A, location 1 is referred to as the ventral side of the hair array, and location 2 is referred to the dorsal side of the hair array.

Fig. 5A] is diverted around the antennule and does not pass through the guard hair array. The mean flow along this ventral edge is $3.6\pm0.3\,cm\,s^{-1}$. Along the opposite, dorsal edge of the aesthetasc hair array [labeled as (2) in Fig. 5A], flow is perpendicular to and out of the guard hair array with a mean flow of $1.1\pm0.2\,cm\,s^{-1}$.

Within the zig-zag pattern of the aesthetasc hair array, the highest flow occurs near the tips of the hairs, with peak velocities of $1.4\,cm\,s^{-1}$. Further within the aesthetasc array, the magnitude of the flow depends upon the proximity to the rows of aesthetasc hairs. Averaged over the entire length of the hair array, the mean flow is $0.24\pm0.06\,cm\,s^{-1}$. During the return stroke (Fig. 5B) the average flow within the aesthetasc hair array is $0.01\pm0.005\,cm\,s^{-1}$, allowing for essentially zero net transport of fluid out of the hair array during the time period of the return stroke. No net flow occurs along the ventral side of the guard hairs due to the combined effect of flow blocking by the antennule and guard hairs. The only flow within the region encompassed by the guard hair array occurs along the dorsal edge, with a magnitude of $0.9\pm0.1\,cm\,s^{-1}$.

Owing to the zig-zag pattern of the aesthetasc hair array, the velocity structure during a flick appears non-uniform along a transect that is perpendicular to the antennule (Fig. 6). The 3D geometry is angled, however, such that the pattern of the zig-zag alternates from the base to the tip, i.e. the zig-zag pattern is arranged so that locations with open gaps at the base of the hairs have closed gaps at the tips, and *vice versa*. Fluid flow within the hair array forms a boundary layer with highest flow that coincides along the center of the gaps and the slowest flow coincides with regions that are adjacent to the rows of hairs (Fig. 7). Within the interior of the aesthetasc array, a uniform velocity of $0.24\pm0.1\,cm\,s^{-1}$ occurs at the center of the gaps between the rows of hairs, whereas adjacent to the hairs viscous interaction reduces the magnitude of flow to $0.10\pm0.06\,cm\,s^{-1}$. Near the tips of the hairs, flow increases both along the gaps and adjacent to the hairs.

Effects of flick and return velocities on flow within the aesthetasc array

The effect of Reynolds number on flow through the hairs was examined by towing the model at Re other than the natural flicking Re. When the antennule is flicked at a rate equivalent to the return stroke (i.e. $Re=0.5$), the mean velocity within the aesthetasc array is $0.012\pm0.005\,cm\,s^{-1}$, whereas for a $Re=1.0$, the average velocity is $0.027\pm0.01\,cm\,s^{-1}$ (Fig. 8). Using the mean width across the aesthetasc hair array of $230\,\mu m$ (Goldman and Koehl, 2001), a simple multiplication of the mean flick speed by the duration of the flick indicates that this flick duration would need to be $1.9\,s$ for a $Re=0.5$ and $0.8\,s$ for a $Re=1.0$ flick to fully exchange the water mass contained within the hair array. This compares with $0.1\,s$ for a natural flick at $Re=2.0$. The distance over which the antennule would need to flick over this time period to completely exchange the entrained fluid would be 4.1 and $3.5\,cm$ for the $Re=0.5$ and 1 flick, respectively. Using a value of $0.24\pm0.06\,cm\,s^{-1}$, measured for the natural flicking $Re=2.0$, an excursion length of $0.8\,cm$ is needed. This is similar to the actual measured flick distance of *P. argus* of between $0.7\,cm$ (Goldman and Patek, 2002) and $0.87\pm0.05\,cm$ (Gleeson et al., 1993). For flicking speeds faster than $Re=2$, flow within the hair array increases dramatically, more than doubling the within-array velocity to $>0.5\,cm\,s^{-1}$ for $Re=2.5$. For a flicking regime of $Re=2.5$, if the
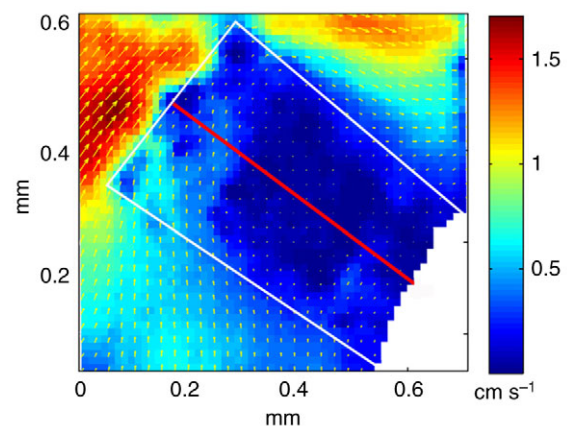

Fig. 6. Magnified view of PIV velocity measurements relative to the aesthetasc array during a flick downstroke (details described in Fig. 5). Flick direction is from right to left. The velocity transects shown in Fig. 7 were taken along the mid-line of the aesthetasc array (highlighted in red). The surrounding white box indicates the location of the aesthetasc hair array.
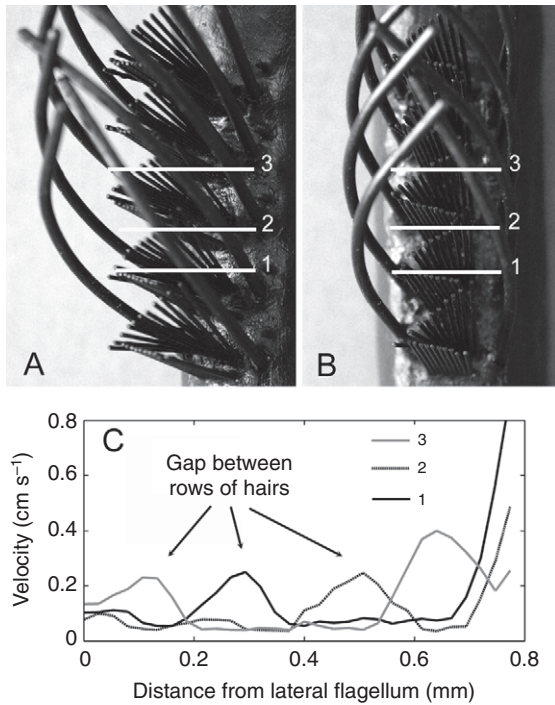
Fig. 7. (A) Side and (B) ventral view of a model of the midsection of the lateral flagellum of a *P. argus* antennule, which has been painted black so that the zig-zag arrangement of the aesthetascs can be easily seen. Lines labeled 1–3 indicate three locations where velocity transects were taken at right angles to the surface of the antennule flagellum, with corresponding velocity measurements shown in graph in C. In total, 20 transects were made at different locations through the aesthetasc array. All distances and velocities have been converted to those for a real antennule. A distance of 0 mm corresponds to the base of the aesthetascs next to the lateral flagellum of the antennule; 0.8 mm corresponds to the tips of the aesthetascs. High flow occurs both near the tips of the aesthetascs and at specific locations within the array where gaps in the zig-zag hair arrangement occur.
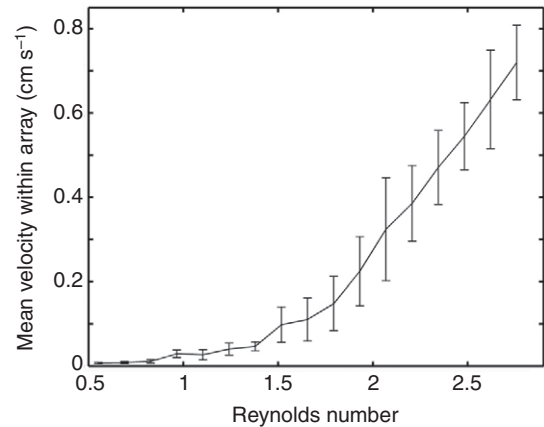

Fig. 8. Mean velocity of fluid within the aesthetasc hair array as a function of Reynolds number (calculated using aesthetasc diameter; *L*). The natural flick occurs at a *Re*=2. Twenty velocity transects were obtained at different locations within the aesthetasc array (as shown in Fig. 7). Mean velocity was computed as the area-averaged velocity along the mid-line of the 20 transects. Error bars indicate one standard deviation.

antennule were to hold constant the distance over which it flicked its antennule, more than twice the amount of fluid exchange would occur within the array than would be necessary to capture a distinct, new parcel of water.

The return stroke occurs at a *Re* of 0.5 and produces a mean flow within the aesthetasc array of $0.01 \pm 0.005 \, \mathrm{cm \, s^{-1}}$. If the return stroke occurs at the same velocity as the flick, at *Re*=2.0, the mean flow is $0.06 \pm 0.005 \, \mathrm{cm \, s^{-1}}$. This signifies that the flick generates four times the flow through the aesthetasc hair array than does the return stroke at the same *Re*=2. The difference is primarily due to the orientation of the hair array during the forward and return strokes. During the flick, the hairs are oriented towards the flick direction into the flow, whereas during the return stroke, the hairs are sheltered behind the antennule.

Effects of orientation angle of the aesthetasc array on flow

The aesthetascs are aligned in a ventrolateral position along the antennule at an angle 32° to the main flick direction (schematic shown in Fig. 2B). This angle has been hypothesized to direct fluid flow into the aesthetasc array during the flick (Gleeson et al., 1993). The effect of this angle on flow penetration into the array was quantified by changing the angle of the antennule to 0° with respect to the flick direction (Fig. 9). The peak flow at the center of the

gaps within the hair array is $0.07 \pm 0.03 \, \mathrm{cm \, s^{-1}}$, with an average flow of $0.03 \pm 0.01 \, \mathrm{cm \, s^{-1}}$ near the rows of aesthetascs. This is a 3.5-fold reduction in velocity through the aesthetasc hair array compared to the realistic 32° orientation. At a 0° orientation, flow along the tips of the aesthetasc array is of similar or slightly greater magnitude than the 32° orientation, but the flow does not penetrate into the interior of the array and no flow occurs along the distal end of the hairs where they attach to the antennule.

Effects of guard hairs

To determine the effect of guard hairs on flow within the aesthetasc array, the hairs were removed from the model and towed in the flick and return orientation. During the downward flick, the mean peak velocity through the aesthetasc hair array without the guard hairs is $0.89 \pm 0.12 \, \mathrm{cm \, s^{-1}}$. This is a 3.7-fold increase in velocity compared to when the guard hairs are in place. Outside of the aesthetasc array but within the region that the guard hairs would normally occupy, the velocity increases from 4.2 to $8 \, \mathrm{cm \, s^{-1}}$ by removing the guard hairs. During the return stroke, the mean peak velocity through the aesthetasc array is $0.025 \pm 0.001 \, \mathrm{cm \, s^{-1}}$ without the guard hairs, an increase of 2.5 times compared to flow when the guard hairs are present. The smaller increase in flow during the return *versus* the flick stroke without the guard hairs is probably due to the blocking effect that the antennule has when the aesthetascs are in the downstream wake of the antennule during the return.

Flow dynamics at mechanosensors

Mechanosensory hairs (labeled '2' in Fig. 1B) line laterally along the antennule, along both the ventral and dorsal outer edges of the guard hairs. PIV analysis of the flow along the ventral side (near location '1' in Fig. 5A) indicates that the mechanosensory hairs are exposed to a mean velocity of $3.9 \pm 0.3 \, \mathrm{cm \, s^{-1}}$ during a flick, while during the return the mean velocity is $0.04 \pm 0.01 \, \mathrm{cm \, s^{-1}}$. Thus, a tenfold variation in flow occurs at the mechanosensory hairs lining the ventral edge of the antennule. Along the dorsal side (near location '2' in Fig. 5A) during the forward flick, the mechanosensory hairs are exposed to a velocity of $0.8 \pm 0.2 \, \mathrm{cm \, s^{-1}}$, whereas during the return, a mean velocity of $1.0 \pm 0.1 \, \mathrm{cm \, s^{-1}}$ is encountered. These velocities act in opposite direction depending on the direction of antennule
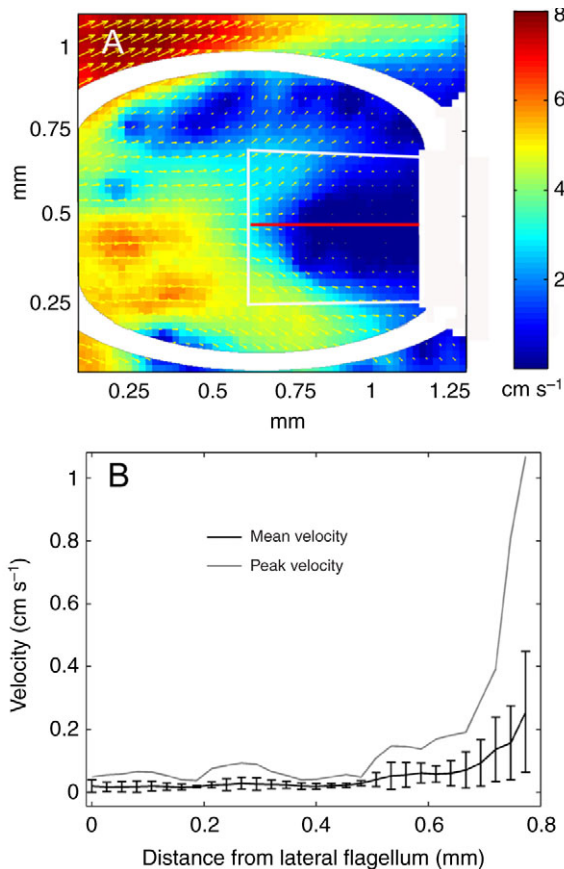
Fig. 9. (A) PIV measurements of water velocities relative to the aesthetascs of a dynamically scaled model of the lateral flagellum of the antennule of a *P. argus* during a flick downstroke (from right to left, details described in Fig. 5). The aesthetascs in this case point in the same direction as antennule motion, rather than being oriented 32° from the direction of the oncoming flow relative to the antennule (see Fig. 2). (B) Peak velocity along the mid-line of the aesthetasc array (transect shown in red) and the mean velocity. Mean velocity was computed as the area-averaged velocity for the 20 transects made through the array. Peak velocity was the maximum velocity measured at a given distance from the lateral flagellum along any of the transects.

movement, but the magnitude of the velocity is essentially the same at this dorsal location. This is due to the offset orientation of the aesthetascs, which shelters the mechanosensory hairs from the main flow during the downward flick, but exposes the mechanosensors to flow during the upstroke phase.

If comparisons are made along the opposite dorsal–ventral sides of the antennule where mechanical sensors are located, the kinematics of the flick creates a fivefold difference in the flow rate. If the *Re* of the downward flick stroke is changed from a *Re*=2 to *Re*=1, the flow rate on the ventral side is $1.15\pm0.1\,\mathrm{cm\,s^{-1}}$, while on the dorsal side, the velocity is $0.1\pm0.03\,\mathrm{cm\,s^{-1}}$. This increases the relative difference between the two locations to almost 12 times. Therefore, because of the orientation of the aesthetasc array, variations in flick speed not only create differences in flow along the aesthetasc array, but also cause changes in flow gradients across the aesthetasc array.

DISCUSSION
Flick *versus* return response

A scaled model of the lateral flagellum of a *P. argus* lobster antennule was used to study the kinematic and morphologic effects

of antennule flicking on fluid transport within the aesthetasc chemosensory hair array. These experiments found that during the fast downstroke of the flick, fluid passes through the chemo-sensitive hair array at a mean velocity of $0.24\,\mathrm{cm\,s^{-1}}$. Owing to the zig-zag geometry of the hair array and the 32° offset angle of the hairs with respect to flick direction, water passes uniformly through the majority of the array, with an increased flow found only near the tips of the aesthetascs. The benefit of this uniform flow is that the distribution of the odors and the concentration sampled during the flick is not appreciably altered during the flick and the odors remain virtually unstirred during the slower return stroke. The distribution of odors across the antennule has been suggested to contain important information for determining source location of the odor (Atema, 1996; Crimaldi et al., 2002; Koehl et al., 2001). This uniform flow distribution is significantly different from that found in stomatopods (Mead and Koehl, 2000), whose antennules consist of four rows of three aesthetascs aligned at a 45° angle to the antennular flagellum. During a stomatopod flick, the main flow penetration into the aesthetasc array occurs at the tip, while a substantial reduction of flow occurs near the base of the aesthetasc array. The majority of dendritic segments where the chemoreceptors reside on the stomatopod aesthetascs are found along the distal portion of the aesthetasc near the tips, in the region where largest flow occurs (Mead and Weatherby, 2002). This is in contrast to the lobster aesthetasc, where the dendritic segments are found over 80% of the length of the hairs. Our measurements on the dynamically scaled model indicate that the morphology of the *P. argus* antennule allows for increased fluid flow near the base of the hairs, essentially allowing for a greater surface area available for chemoreception. The added benefit of this uniform flow is that the physical and temporal structure of the filaments of odor formed during turbulent transport within the ambient fluid is not altered significantly when encountered by a flicking antenna (Koehl et al., 2001).

Gleeson et al. (Gleeson et al., 1993) measured the mean duration of a flick to be $113\pm3\,\mathrm{ms}$, with the mean excursion distance (as measured from the center of the aesthetasc tuft) of $8.7\pm0.5\,\mathrm{mm}$. Measurements obtained on the scaled model indicate that average distance over which fluid travels in the aesthetasc array is $0.27\,\mathrm{mm}$ if one multiplies the average velocity of the water within the hair array by the duration of a flick. This value is just larger than the average width of the aesthetasc row measured at both the base and the tip of the hair array, of $0.23\pm0.02\,\mathrm{mm}$ and $0.22\pm0.03\,\mathrm{mm}$, respectively (Goldman and Koehl, 2001), indicating that during each flick, the entirety of the fluid held within the hair is exchanged with new fluid. Kinematic variation of the model has shown that flicking faster or longer exchanges appreciably more fluid than is necessary to obtain a discrete new sample of fluid, whereas a slower or shorter flick would not allow for a complete exchange of fluid within the array.

Since a flicking flagellum rotates relative to a fixed point at the base of the antennule, the velocity of the flick will vary linearly along the length of the flagellum. Our model was towed at a velocity and *Re* encountered at the midpoint of the aesthetasc hair-bearing region along the antennule. Locations distal from this location should experience relatively faster flicking speeds, while locations closer to the base of the antennule should experience slower speeds with respect to the ambient flow. Goldman and Koehl (Goldman and Koehl, 2001) also reported that the tip of the antennule bends as it is moved through the water such that the relative speed may be faster or slower than the mid-point of the antennule at a given instant during the flick. They measured peak speeds of the tip of the antennule to be $0.12\,\mathrm{m\,s^{-1}}$, compared with peak speeds at the mid-

point of $0.09\,\mathrm{m\,s^{-1}}$. This increase in speed will increase the *Re* for a constant aesthetasc hair array geometry. However, the antennule tapers near the tip. Although measurements have not been performed to determine if changes in antennule diameter also scale with changes to the morphology of the aesthetasc hair array near the tip, Gleeson et al. (Gleeson et al., 1993) found that the guard hair spacing does scale geometrically with antennule width across a range of *P. argus* carapace sizes. Whether the increase in flicking speed at the tip is offset by a decrease in antennule width and thus a corresponding change in aesthetasc hair geometry to keep *Re* constant is still unknown.

Importance of morphology to odor sampling

We tested the effects of the guard hairs on fluid transport by removing the hairs from the antennule model. When this was done, the transport of water through the aesthetasc array increases to 3.7 times higher than when guard hairs were present. The guard hairs apparently have the dual role of protecting the aesthetasc array from damage as well as conditioning the flow to allow for the correct 'leakiness' during a flick and return sequence. During the return stroke, with the absence of guard hairs the mean flow through the aesthetasc array increases 2.5 times. The less pronounced increase during the return is due primarily to the sheltering of the aesthetasc hairs, which are oriented downstream in the wake of the antennule during the return stroke.

Altering the orientation of the hair array from a 32° to a 0° offset orientation with respect to flick direction increased flow along the tips of the aesthetascs, but reduced flow penetration into the array. With the 32° orientation, flow along the ventral side of the array was diverted to penetrate perpendicularly into the zig-zag orientation of the aesthetascs, allowing fluid to infiltrate more uniformly along the length of the aesthetasc hairs. At a 0° orientation, flow was diverted around the aesthetascs near the tips and never penetrated appreciably into the inner region, reducing the ability for odor molecules entrained in the fluid to come into contact with the chemosensory surfaces of the hairs.

Odor transport to chemosensory hairs

Flow adjacent to the rows of aesthetasc hairs was less than half that measured along the centerline of the gaps found between the hairs. This reduction of flow caused by frictional interaction with the hairs, forming a boundary layer, limits odor transport to the chemosensory cells lining the aesthetascs. However, the slower return stroke, and pause before the next flick, allows odor molecules time to diffuse to the surfaces of the aesthetascs. During the return stroke, the average velocity within the hair array was measured to be $0.01\,\mathrm{cm\,s^{-1}}$, and no variation in velocity was measured with respect to location within the array. Goldman and Koehl (Goldman and Koehl, 2001) measured the average duration of a return stroke plus pause period before the next flick occurs to be much more variable than the downward flick stroke. The return stroke plus pause period lasted between 0.20 and 0.90 s. Under such low flow conditions, it is hypothesized that the main mechanism for odor transport to the sensory cells along the aesthetasc hair array is by molecular diffusion (Koehl, 2001; Stacey et al., 2002). Most odors that attract lobsters are composed of amino acids with a molecular diffusivity (*D*) of $10^{-9}\,\mathrm{m^2\,s^{-1}}$ (Lide, 1991). The average root mean squared distance (x_{rms}) odor molecules would molecularly diffuse over time *t* would be $x_{rms} = \sqrt{2Dt}$ (Denny, 1993). If 0.5 s is assumed as the mean duration of the return stroke, an odor molecule travels on average $32\,\mu\mathrm{m}$ over the time period of the return stroke plus pause. The average spacing between arrays of aesthetasc hairs of an adult *P.*

argus lobster (Goldman and Koehl, 2001) was measured to be $53\,\mu\mathrm{m}$ at its narrowest and $196\,\mu\mathrm{m}$ at its widest location, with a mean gap width of $125\,\mu\mathrm{m}$. This indicates that given a uniform distribution of odor molecules, up to 25% of the odor molecules entrained within the hair array should be molecularly fluxed to the aesthetasc surfaces during the time period of the return stroke.

Lobsters in their natural habitats are exposed to ambient water flow. Although flicking behavior of *P. argus* exposed to ambient water currents has not yet been quantified, such behavior has been studied in the stomatopod, *Hemisquilla ensiguera*. *Hemisquilla* changed the velocity of their flicking so that the net water velocity relative to the tip of their antennule (the vector sum of the ambient current and the water flow past the antennule tip due to flicking) maintained the *Re* of the rapid stroke of the flick (K. S. Mead, personal communication). Blue crabs, *Callinectes sapidus*, when exposed to ambient flow that exceeded the speed of their flick, ceased flicking and simply extended their antennules with the aesthetascs facing into the main direction of flow (M. Martinez, U. Lee and M.A.R.K., unpublished).

Integration of hydrodynamic and odorant signals

Crabs, lobsters and crayfish all detect odorants using antennules that bear both chemoreceptive and mechanoreceptive sensilla (Steullet et al., 2002; Mellon, 2005; Mellon, 2007). Much work has been done on the neurobiology of chemoreception in lobsters (reviewed by Schmidt, 2007), and recent studies have begun exploring how olfactory and hydrodynamic signals are processed and integrated in the brain (Mellon, 2007). For example, research on crayfish has shown that initiation of water movement past the antennular lateral flagellum evokes responses in the crayfish brain that enhance the chemosensory signal (Mellon and Humphrey, 2007), indicating that multimodal integration of chemical and mechanical information occurs in the neurons of the crayfish brain. Our measurements of water velocities relative to the mechanosensory hairs along the sides of the lateral flagellum of the *P. argus* antennule show distinct differences between the flow they encounter during the rapid flick downstroke, and the slower return stroke. Rapid water motion past the mechanoreceptors on the lateral flagellum of the antennule during each flick downstroke can serve as an indicator that a new sample of water has just been taken from the environment. Although hydrodynamic studies make it clear that flicking (1) increases the rates at which odorant molecules reach chemosensory sensilla, and (2) permits the animal to take odor samples that are discrete in space and time, further research is still needed to determine the extent to which hydrodynamic and olfactory sensory modalities are combined to affect both the neurobiology and behavior of lobsters when detecting odors in natural environments.

LIST OF ABBREVIATIONS

D	molecular diffusivity
L	characteristic dimension of the structure (e.g. aesthetasc diameter)
v	kinematic viscosity of the fluid
PIV	particle image velocimetry
Re	Reynolds number
t	time
U	velocity of the fluid
x_{rms}	root mean square distance
y	distance to the tank wall

REFERENCES

Atema, J. (1996). Eddy chemotaxis and odor landscapes: exploration of nature with animal sensors. *Biol. Bull.* **191**, 129-138.

Cheer, A. Y. L. and Koehl, M. A. R. (1987). Fluid flow through filtering appendages of insects. *IMA J. Math. Appl. Med. Biol.* **4**, 185-199.

Cowen, E. A. and Monismith, S. G. (1997). A hybrid digital particle tracking velocimetry technique. *Exp. Fluids* **22**, 199-211.

Crimaldi, J. P. and Koseff, J. R. (2001). High resolution measurements of the spatial and temporal scalar structure of a turbulent plume. *Exp. Fluids* **31**, 90-102.

Crimaldi, J. P., Koehl, M. A. R. and Koseff, J. R. (2002). Effects of the resolution and kinematics of olfactory appendages on the interception of chemical signals in a turbulent odor plume. *Environ. Fluid Mech.* **2**, 35-63.

Denny, M. W. (1993). *Air and Water.* Princeton, NJ: Princeton University Press.

Gleeson, R. A., Carr, W. E. S. and Trapido-Rosenthal, H. G. (1993). Morphological characteristics facilitating stimulus access and removal in the olfactory organ of the spiny lobster, *Panulirus argus*: insight from the design. *Chem. Senses* **18**, 67-75.

Goldman, J. A. and Koehl, M. A. R. (2001). Fluid dynamic design of lobster olfactory organs: high speed kinematic analysis of antennule flicking by *Panulirus argus*. *Chem. Senses* **26**, 385-398.

Goldman, J. A. and Patek, S. N. (2002). Two sniffing strategies in palinurid lobsters. *J. Exp. Biol.* **205**, 3891-3902.

Grunert, U. and Ache, B. W. (1988). Ultrastructure of the aesthetasc (olfactory) sensilla of the spiny lobster *Panulirus argus*. *Cell Tissue Res.* **251**, 95-103.

Horner, A., Weissburg, M. and Derby, C. (2007). The olfactory pathway mediates sheltering behavior of Caribbean spiny lobsters, *Panulirus argus*, to conspecific urine signals. *J. Comp. Physiol. A Neuroethol. Sens. Neural. Behav. Physiol.* **194**, 243-253.

Johnson, M. E. and Atema, J. (2005). The olfactory pathway for individual recognition in the American lobster *Homarus americanus*. *J. Exp. Biol.* **208**, 2865-2872.

Keller, T. A., Powell, I. and Weissburg, M. J. (2003). Role of olfactory appendages in chemically mediated orientation of blue crabs. *Mar. Ecol. Prog. Ser.* **261**, 217-231.

Koehl, M. A. R. (1995). Fluid flow through hair-bearing appendages: feeding, smelling and swimming at low and intermediate Reynolds numbers. *Symp. Soc. Exp. Biol.* **49**, 157-182.

Koehl, M. A. R. (2001). Fluid dynamics of animal appendages that capture molecules: arthropod olfactory antennae. In *Computational Modeling in Biological Fluid Dynamics* (ed. L. J. Fauci and S. Gueron). New York: Springer-Verlag.

Koehl, M. A. R. (2006). The fluid mechanics of arthropod sniffing in turbulent odor plumes. *Chem. Senses* **31**, 93-105.

Koehl, M. A. R., Koseff, J. R., Crimaldi, J. P., McCay, M. G., Cooper, T., Wiley, M. B. and Moore, P. A. (2001). Lobster sniffing: Antennule design and hydrodynamic filtering of information in an odor plume. *Science* **294**, 1948-1951.

Lide, D. R. (1991). *CRC Handbook of Chemisty and Physics.* Boca Raton, FL: CRC Press.

Loudon, C., Best, B. A. and Koehl, M. A. R. (1994). When does motion relative to neighboring surfaces alter the flow through arrays of hairs? *J. Exp. Biol.* **193**, 233-254.

Mead, K. S. and Koehl, M. A. R. (2000). Stomatopod antennule design: The asymmetry, sampling efficiency, and ontogeny of olfactory flicking. *J. Exp. Biol.* **203**, 3795-3808.

Mead, K. S. and Weatherby, T. M. (2002). Morphology of stomatopod chemosensory sensilla facilitates fluid sampling. *Invertebr. Biol.* **121**, 148-157.

Mead, K. S., Koehl, M. A. R. and O'Donnell, M. J. (1999). Stomatopod sniffing: the scaling of chemosensory sensillae and flicking behavior with body size. *J. Exp. Mar. Biol. Ecol.* **241**, 235-261.

Mellon, D. (2005). Integration of hydrodynamic and odorant inputs by local interneurons in the crayfish deutocerebrum. *J. Exp. Biol.* **208**, 3711-3720.

Mellon, D. (2007). Combining dissimilar senses: Central processing of hydrodynamic and chemosensory inputs in aquatic crustaceans. *Biol. Bull.* **213**, 1-11.

Mellon, D. and Humphrey, J. A. (2007). Directional asymmetry in responses of local interneurons in the crayfish deutocerebrum to hydrodynamic stimulation of the lateral antennular flagellum. *J. Exp. Biol.* **210**, 2961-2968.

Moore, P. and Crimaldi, J. P. (2004). Odor landscapes and animal behavior: tracking odor plumes in different physical worlds. *J. Mar. Sys.* **49**, 55-64.

Moore, P. A., Atema, J. and Gerhardt, G. A. (1991). Fluid dynamics and microscale chemical movement in the chemosensory appendages of the lobster, *Homarus americanus*. *Chem. Senses* **16**, 663-674.

Rahman, S. and Webster, D. R. (2005). The effect of bed roughness on scalar fluctuations in turbulent boundary layers. *Exp. Fluids* **38**, 372-384.

Schlichting, H. and Gersten, K. (2000). *Boundary Layer Theory.* New York: Springer-Verlag.

Schmidt, M. (2007). The olfactory pathway of decapod crustaceans – an invertebrate model for life-long neurogenesis. *Chem. Senses* **32**, 365-384.

Schmidt, M. and Derby, C. (2005). Non-olfactory chemorecptors in asymmetric setae activate antennular grooming behavior in the Caribbean spiny lobster *Panulirus argus*. *J. Exp. Biol.* **208**, 233-248.

Schmitt, B. C. and Ache, B. W. (1979). Olfaction: responses of a decapod crustacean are enhanced by flicking. *Science* **205**, 204-206.

Schoenfeld, T. A. (2006). Introduction to special issue: What's in a sniff? *Chem. Senses* **31**, 91-92.

Stacey, M. T., Mead, K. S. and Koehl, M. A. R. (2002). Molecule capture by olfactory antennules: Mantis shrimp. *J. Math. Biol.* **44**, 1-30.

Steullet, P., Krützfeldt, D. R., Hamidani, G., Flavus, T., Ngo, V. and Derby, C. (2002). Dual antennular chemosensory pathways mediate odor-associative learning and odor discrimination in the Caribbean spiny lobster *Panulirus argus*. *J. Exp. Biol.* **205**, 851-867.

Sven, J. K. (2004). *An introduction to MatPIV v. 1.6.1.:* Mechanics and Applied Mathematics. vol. 2. Oslo: Dept. of Mathematics, University of Oslo.

Vogel, S. (1994). *Life in Moving Fluids: The Physical Biology of Flow.* Princeton, NJ: Princeton University Press.

Webster, D. R. and Weissburg, M. J. (2001). Chemosensory guidance cues in a turbulent chemical odor plume. *Limnol. Oceanogr.* **46**, 1034-1047.

Webster, D. R., Rahman, S. and Dasi, L. P. (2001). On the usefulness of bilateral comparison to tracking turbulent chemical odor plumes. *Limnol. Oceanogr.* **46**, 1048-1053.